JOURNAL OF CATALYSIS 122, 95–112 (1990)

On Kinetic Phase Transitions in Surface Reactions

MARTINE DUMONT,[1] P. DUFOUR, B. SENTE, AND R. DAGONNIER

Faculté des Sciences, Université de l'Etat, B-7000 Mons, Belgium

Received July 29, 1988; revised April 20, 1989

The steady-state properties for the bimolecular surface reaction $A + \frac{1}{2}B_2 \rightarrow AB$ are investigated. Kinetic phase transition points, bistability, and hysteresis characteristics are specified by using kinetic equations of the mean-field-approximation type. Comparisons with Monte Carlo simulation results are made. © 1990 Academic Press, Inc.

1. INTRODUCTION

Surface reactions when operating as open systems behave as nonequilibrium systems (*1*). They show *kinetic* (or *nonequilibrium*) phase transitions, bistability and associated hysteresis, complex self-sustained oscillations, and dissipative structures like propagating waves of temperature and concentration (*2*).

Most oxidation reactions catalysed by metals of the Pt group exhibit such properties (*3*). These reactions have a main feature in common: they involve a competitive coadsorption of two reactants sharply different in their redox properties. The most thoroughly studied surface reaction of this type is the catalytic CO oxidation (*4*). Bistability of the oxidation rate under stationary conditions (steady-state hysteresis) has been observed (*5*). The two branches of the reaction rate coalesce at a point where self-oscillations are observed (*4*).

These CO oxidation rate oscillations have been tentatively described by a bewildering variety of kinetic models involving nonlinearities of different nature (see the review by Razon and Schmitz (*4*), Table 3 of which refers to about a hundred models!). The prescription includes in the kinetic scheme some steps which sequentially exert a reversible feedback on the catalytic properties of the surface (*6*). Depending on the pressure conditions, two models of current interest for *isothermal* self-oscillations should be mentioned.

In their study of the CO oxidation *at low pressure* ($\leq 10^{-4}$ Torr) on Pt(100) crystals, Ertl and co-workers (*7*) have derived a model which couples the rate oscillations with a reversible surface structural transition hex $\leftrightarrow$ (1 × 1). The two phases exhibit different adsorption properties of the reactants. *At higher pressure* (>1 Torr) the most common interpretation for these oscillations is supported by the STM (Sales–Turner–Maple) model (*8–10*) which involves a coupling of the reaction with a reversible metal oxidation $\leftrightarrow$ reduction step. The reactivity on the surface Pt oxide is different from that on the metal.

As a companion process of this self-oscillating behaviour we should mention the reaction rate resonances observed when the reaction operates under feed concentration cyclic forcing. Under such periodic boundary conditions the time averaged reaction rate can be very much larger than the maximum possible steady-state reaction rate at the same temperature (*11–13*).

A detailed description of these twin dynamical behaviours should feature a theoretical investigation of the possible kinetic phase transitions exhibited by the adsorbate under the influence of the bifurcating parameters involved in the problem.

[1] Research Associate, National Fund for Scientific Research (Belgium).

0021-9517/90 $3.00
Copyright © 1990 by Academic Press, Inc.
All rights of reproduction in any form reserved.

The objective of this paper is the analysis of the bifurcation diagrams corresponding to kinetic schemes modelling a CO oxidation type reaction. These phase diagrams are obtained either by solving kinetic equations derived on the basis of statistical mechanics arguments or, more directly, from Monte Carlo simulations (MCS) (*14*).

We consider the bimolecular surface reaction

$$A + \tfrac{1}{2}B_2 \xrightarrow{\text{catalytic surface}} AB \qquad (1)$$

described, as a start, by the simple *irreversible* model:

$$A + S \xrightarrow{1} AS \qquad (2.1)$$

$$B_2 + S_2 \xrightarrow{2} 2BS \qquad (2.2)$$

$$AS + BS \xrightarrow{3} AB + S_2, \qquad (2.3)$$

where S denotes a vacant site, S_2 stands for a vacant *dual* site, i.e., a pair of nearest-neighbour empty sites.

We also show how the bifurcation diagram of the basic model (Eqs. (2.1)–(2.3)) is modified by the inclusion of the desorption of molecules A (a bit of reversibility),

$$A + S \xleftarrow{-1} AS \qquad (3)$$

and/or the Eley–Rideal mechanism (a second reaction path)

$$A + BS \xrightarrow{4} AB + S. \qquad (4)$$

Both the kinetic equations and the MCS discussed below are based on the following assumptions.

(1) The catalyst surface remains structurally and chemically stable during the reaction.

(2) A and B_2 molecules competitively adsorb on active sites of the same kind and react to product AB molecules via the Langmuir–Hinshelwood (LH) mechanism, Eq. (2.3). The rate constant k_3 of this reaction mechanism is the reciprocal of the reaction time τ_3, i.e., the mean time spent by two adjacent A and B reactants to form the product AB molecule which then desorbs without interacting further with the system.

(3) Any activation energy is coverage independent.

(4) The temperature and flow rate are constant and such that the reaction may be considered as isothermal and kinetically controlled. Heat and mass transfer resistances are absent.

(5) The state variables of the problem are the fractional coverages defined as follows (for a square lattice):

$$X_i = N_i/N,\ X_{ij} = N_{ij}/2N,\ X_{ijk} = N_{ijk}/6N. \qquad (5)$$

$N_i(N_{ij}, N_{ijk})$ stands for the number of sites (dual sites, triplet sites) per unit area occupied by the species i (ij pairs, ijk triplets). N is the total number of active sites per unit area of the catalyst surface.

With these assumptions each step i (of rate R_i) of the irreversible kinetic scheme, Eqs. (2.1)–(2.3), contributes to the following balance equations:

$$dX_A/dt = R_1 - R_3 = k_1X_S - 2k_3X_{AB} \qquad (6.a)$$

$$dX_B/dt = 2R_2 - R_3 = 2k_2X_{SS} - 2k_3X_{AB}. \qquad (6.b)$$

Hereafter subscripts 1 and 2 refer to A (e.g., CO) and B (e.g., oxygen), respectively. The subscript S refers to vacant sites. The rate constants k_i are defined in Section 2.

Although exact, the system of Eqs. (6a) and (6b) is not closed: it conceals a *dynamic hierarchy* connecting "sites" to pairs, pairs to triplets, etc. Indeed, in addition to the obvious relation

$$X_S = 1 - X_A - X_B \qquad (7)$$

we have the sum rules (for a square lattice)

$$X_i = \tfrac{1}{2}[X_{ii} + \sum_j X_{ij}] \qquad (8)$$

$$X_{ij} = [1/(1 + \delta_{ij})][X_{iji} + \sum_k X_{ijk}], \qquad (9)$$

where $\delta_{ij} = 1$ if $i = j$ and zero otherwise.

The cut-off of this hierarchy is usually achieved within the *site*-mean field approximation (*site*-MFA), i.e., assuming that (e.g., Ref. (*15*))

(i) the adsorbed molecules A and B are randomly distributed among the surface sites.

(ii) the occupation state of any site is independent of its neighbourhood.

This *site*-MFA (denoted by the superscript ^{0}) consists of approximating X_{ij} by

$$X_{ij}^0 = [2/(1 + \delta_{ij})]X_i^0 X_j^0. \qquad (10)$$

The *site*-MFA phase transition features of the basic model, Eqs. (2.1)–(3), are presented in Section 2.

In Section 3 we derive *closed* kinetic equations for the pair coverages X_{ij} by applying the same "mean field" concept to dual sites as, here above, to single sites. We assume that the occupation state of any *dual* site is independent of its neighbourhood; i.e., we restrict our description to the nearest neighbour correlations. The idea underlying this *pair*-MFA (*17*) may be found in the Bethe closed form approximation for lattice systems (*18*).

For instance the dissociative adsorption of molecules B_2, Eq. (2.2), increases the coverage X_{AB} as follows

$$\left.\frac{dX_{AB}}{dt}\right|_{(2)} = \frac{k_2}{4N} N_{ASS} \qquad (11)$$

According to this *pair*-MFA, we assume that

$$N_{ASS} = N_{SS} \cdot 6 \cdot P_{S/A} \overset{\text{or}}{=} N_{AS} \cdot 3 \cdot P_{S/S}.$$

Any pair $SS(AS)$ has 6(3) dangling bonds available to form a triplet ASS with a probability $P_{S/A}(P_{S/S})$ per bond. $P_{i/j}$ is the *conditional* probability to meet a *dual* site with one side in state j while the adjacent side is in a given state i:

$$P_{i/j} = N_{ij}/4N_i = X_{ij}/2X_i;$$
$$P_{i/i} = 2N_{ii}/4N_i = X_{ii}/X_i. \qquad (12)$$

Therefore, Eq. (11) becomes

$$\left.\frac{dX_{AB}}{dt}\right|_{(2)} = \frac{3}{2} k_2 X_{SS} X_{AS}/X_S. \qquad (13)$$

Proceedings in this way we derive six *coupled* kinetic equations for X_{ij} (see Appendix A) whose solutions lead to the coverages X_i (see sum rule, Eq. (8)).

Full details of our MCS procedures may be found in Ref. (*14b,c*). Restricting the kinetic scheme to Eqs. (2.1)–(2.3) and (3), we can sketch our MCS as follows.

A random rainfall of molecules A and B_2 is *uniformly* distributed on a square lattice submitted to boundary conditions and empty at the start. We assume the adsorption steps, Eqs. (2.1)–(2.2), to be Poisson processes and therefore, for empty sites, we randomly select the arrival of each molecule A or B_2 on the basis of an *exponential* distribution of average τ_i ($i = 1, 2$):

$$\tau_i = k_i^{-1}, \qquad (14)$$

the nearest event in time being programmed.

Once adsorbed on the lattice a molecule A can desorb or, possibly, react with an adjacent adsorbed partner B. When competitive these processes are selected as for the adsorption processes but with τ_i, Eq. (14), specified accordingly, i.e., for $i = -1$, 3. For the steps $i = 2, 3$ and when necessary the choice between one or another favorable configuration is randomly selected by using a uniform distribution.

In section 4 we present and discuss the main features of the bifurcation diagrams obtained, respectively, within the *site*-MFA, the *pair*-MFA, and by our MCS treatment of reaction, Eq. (1).

Comparisons are also made with results issued from the investigations of the *irreversible* model, Eqs. (2.1)–(2.3), idealized along the rules of Ziff *et al.* (*16*). These authors assume, especially, an *infinite* reaction rate constant k_3 (i.e., $\tau_3 = 0$) and, therefore, the absence of pairs AB on the surface (i.e., $X_{AB} = 0$ always). This assumption

clearly refers to situations where the adsorptions, Eqs. (2.1)–(2.2) may be considered as the rate-limiting steps of the global kinetics. In their MCS of the kinetics of the irreversible model, Ziff *et al.* show that the adsorbate undergoes both a *first-* and a *second*-order kinetic phase transition. These two transition points delimit in control parameter space the domain of existence of a *mixed* adsorbate. Outside this "reactive window" the surface is saturated by a single species and the reaction is totally inhibited. These results are confirmed by the pair-MFA kinetics description proposed by Dickman (*17*) for this model (hereinafter called the ZD model).

In contradistinction to the ZD model, our approach considers, as a rule, a finite reaction rate constant k_3 (i.e., $X_{AB} \neq 0$). Therefore we were able to investigate on a larger scale the bifurcating role of the control parameters on the kinetics of reaction, Eq. (1).

Moreover, in Section 4 we also show how the bifurcation diagram of the irreversible model is modified by (i) the desorption of molecules A, Eq. (3), which induces a steady-state hysteresis, and (ii) the Eley–Rideal mechanism, Eq. (4), which suppresses the second-order kinetic phase transition.

Conclusions are proposed in Section 5 with special attention to the second-order kinetic phase transition which, in the absence of any experimental evidence, remains an artifact of the models so far investigated.

2. SITE MEAN FIELD APPROXIMATION

In the *site*-MFA, Eq. (10), the kinetic equations, Eqs. (6.a) and (6.b) read

$$dX_A^0/dt = R_1^0 - R_3^0 = k_1 X_s^0 - 4k_3 X_A^0 X_B^0 \tag{15.a}$$

$$dX_B^0/dt = 2R_2^0 - R_3^0 = 2k_2 (X_s^0)^2 - 4k_3 X_A^0 X_B^0. \tag{15b}$$

The adsorption rate constants (per site) k_i ($i = 1, 2$) may be written as follows (e.g., Ref. (*15*))

$$k_i = \bar{k}_i p_i = \bar{k}_i P(\eta \delta_{i,1} + \delta_{i,2})/(1 + \eta), \quad i = 1, 2, \tag{16.a}$$

where

$$\bar{k}_i = \sigma_i N^{-1} (2\pi m_i kT)^{-1/2} \exp(-E_i/RT). \tag{16b}$$

p_i, σ_i, and E_i are, respectively, the partial pressure, the condensation coefficient, and the adsorption activation energy. Moreover, η denotes the partial pressure ratio

$$\eta = p_1/p_2, \tag{16.c}$$

and P, the total pressure of the reactants

$$P = p_1 + p_2. \tag{16.d}$$

For future use let us also define the temperature-dependent parameter α_T

$$\alpha_T = \bar{k}_2/\bar{k}_1 = \alpha_\infty \exp[-(E_2 - E_1)/RT], \quad \alpha_\infty = (\sigma_2/\sigma_1)(m_1/m_2)^{1/2} \tag{16.e}$$

and the reaction rate constant k_3

$$k_3 = k_3' \exp(-E_3/RT). \tag{17}$$

Finally, by referring to the CO oxidation (*4*), we shall assume throughout this work that

$$E_3 > E_2 > E_1 \approx 0 \tag{18}$$

The system of Eqs. (15.a) and (15.b) admits four steady-state solutions (denoted by overbars) characterized by the following linear stability signatures (e.g., Ref. (*19b*): two *pure* adsorbates

$$\bar{X}_A^0 = 1, \quad \bar{X}_B^0 = 0; \quad \text{a stable node} \tag{19.a}$$

$$\bar{X}_A^0 = 0, \quad \bar{X}_B^0 = 1; \quad \text{a saddle point} \tag{19.b}$$

and two *mixed* adsorbates

$$\bar{X}_A^0 = \tfrac{1}{2}(1 - \bar{X}_s^0)[1 + \delta], \quad \bar{X}_B^0 = \tfrac{1}{2}(1 - \bar{X}_s^0)[1 - \delta]; \quad \text{a saddle point} \tag{20.a}$$

$$\bar{X}_A^0 = \tfrac{1}{2}(1 - \bar{X}_s^0)[1 - \delta],$$
$$\bar{X}_B^0 = \tfrac{1}{2}(1 - \bar{X}_s^0)[1 + \delta];$$
a stable node, (20.b)

where (see Eqs. (16.a)–(16.e)

$$\bar{X}_s^0 = k_1/2k_2 = \eta/2\alpha_T \quad (21)$$

with

$$0 \le k_1 \le 2k_2, \quad 0 \le \eta \le 2\alpha_T. \quad (22)$$

The quantity δ is the positive square root of

$$\delta^2 = 1 - k_c/k_3, \quad (23)$$

where

$$k_c = k_1\bar{X}_s^0/(1 - \bar{X}_s^0)^2. \quad (24)$$

Let us now consider the main steady-state features of the irreversible model, Eqs. (2.1)–(2.3), treated in the site-MFA. Comparisons should be made with experiments performed in a temperature range where the desorption of A (and a fortiori of B_2) is negligible.

(1) The steady-state total adsorbate coverage (use Eqs. (7) and (21))

$$\bar{X}_A^0 + \bar{X}_B^0 = 1 - k_1/2k_2 = 1 - \eta/2\alpha_T \quad (25)$$

as well as the steady-state reaction rate (use Eqs. (21) and (16.a)–(16.e))

$$\bar{R}_3^0 = \bar{R}_1^0 = k_1\bar{X}_s^0$$
$$= k_1^2/2k_2 = \bar{k}_1 P\eta^2/2\alpha_T(1 + \eta) \quad (26)$$

do not depend on the reaction rate constant k_3. This drawback, clearly due to the *site*-MFA

$$\bar{X}_{SS}^0 = (\bar{X}_S^0)^2 \quad (27)$$

has as consequences that the reaction rate should decrease slightly when T increases (at P and η fixed) and be parabolic in the limit $\eta \to 0$ (at P and T fixed). These features are not confirmed by the experiments (*5*).

(2) The reaction leads to a stable steady mixed adsorbate (richer in B) provided (see Eqs. (20.b) and (23))

$$k_3 > k_c. \quad (28)$$

Note that in the *site*-MFA the surface can be "poisoned" by $B(\bar{X}_A^0 = 0, \bar{X}_B^0 = 1)$ only in the limit $\delta \to 1$, i.e., practically, when η goes to zero. We shall see later that the *pair*-MFA as well as MCS of the model shows that this *second-order* (i.e., continuous) kinetic phase transition occurs at a *finite* value of η.

(3) A *first-order* (i.e., discontinuous) kinetic phase transition between an equally distributed stable adsorbate ($\bar{X}_A^0 = \bar{X}_B^0 = (1 - \bar{X}_S^0)/2$) and a stable pure A-adsorbate ($\bar{X}_A^0 = 1$, $\bar{X}_B^0 = 0$) occurs when (see Eqs. (20) and (23))

$$k_3 = k_c \quad (29)$$

or, explicitly (use Eqs. (24), (21), and (16.a)–(16.e)) when

$$\eta^3 + (1 - 4\alpha_T - 2\alpha_T\bar{k}_1 P/k_3)\eta^2$$
$$- 4\alpha_T(1 - \alpha_T)\eta + 4\alpha_T^2 = 0. \quad (30)$$

The first-order phase transition (see Fig. 1) occurs for appropriate values of three *external* parameters; namely, the reactant total pressure P, Eq. (16.d), the partial pressure ratio η, Eq. (16.c), and the ambient temperature T. Eq. (30), together with Eq. (22), shows the subtle role of P, η, and T as *bifurcating* parameters of the problem.

At this critical point, Eq. (29), the system switches from the reactive phase, where the reaction rate is maximum

$$\bar{R}_3^0 = k_1\bar{X}_S^0 = k_c(1 - \bar{X}_S^0)^2 \quad (31)$$

to an *inhibited* phase ("poisoned" by A).

In experiments, this first-order transition point corresponds to the sudden transition, in the control parameters space (P, η, T), of the (maximum) self-oscillation regime to its extinction. This transition is commonly observed in the catalytic CO oxidation (*4*, *5*). Depending on the experimental conditions this critical point undergoes *relative* shifts which can be interpreted in the site-MFA as follows.

If we note that the *critical* constant k_c, Eq. (24), behaves as follows (use Eqs. (21) and (16.a)–(16.e))

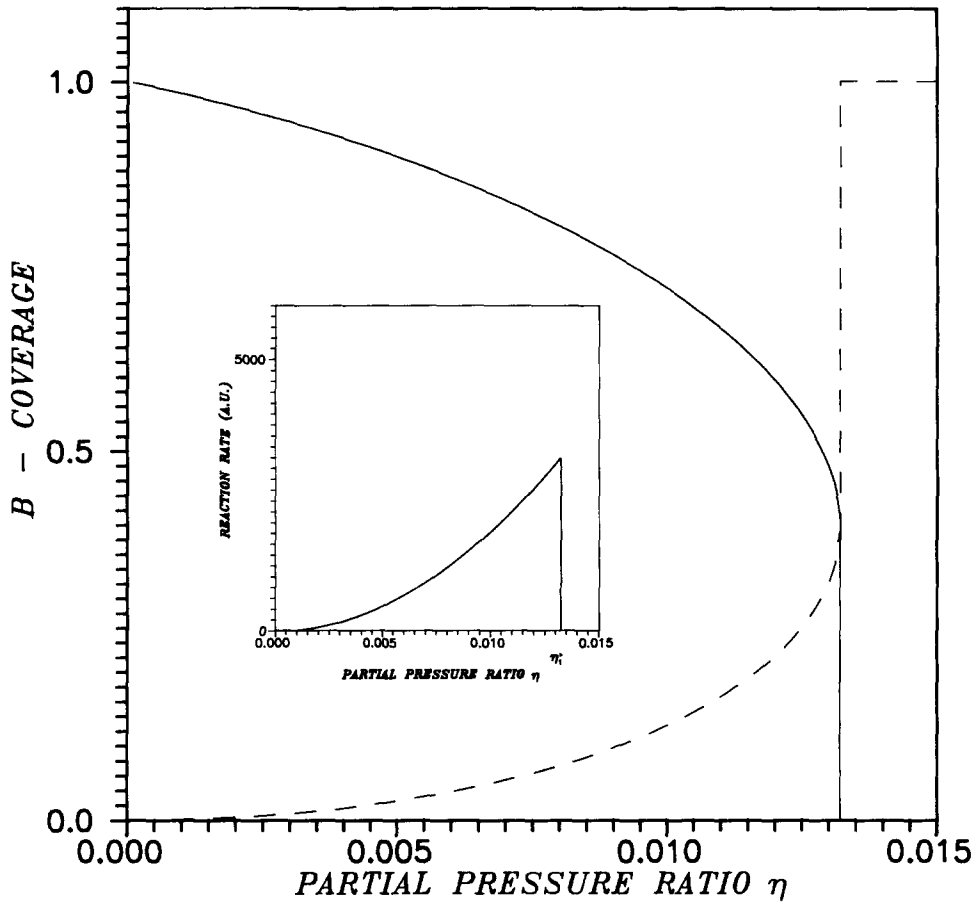

FIG. 1. *Site*-MFA bifurcating diagram corresponding to the steady-state mixed adsorbates, Eqs. (20.a) and (20.b). Here $k_3 = 10^6\ s^{-1}$, $P = 1$ atm, and $T = 500$ K (see Eqs. (48a)–(48c)). The solid line corresponds to the stable (resp. unstable) coverages $\overline{X}_B^0$ (resp. $\overline{X}_A^0$); the dashed line corresponds to the unstable (resp. stable) coverage $\overline{X}_B^0$ (resp. $\overline{X}_A^0$). The first-order transition occurs for $\eta = \eta_1^> = 0.0132$ (see Eq. (30)). The inset shows the corresponding steady-state reaction rate $\overline{R}_3^0$, Eq. (26).

$$k_c = PF(\eta, T) \tag{32.a}$$

with

$$(\partial F/\partial \eta)_T > 0 \tag{32.b}$$

and

$$(\partial F/\partial T)_\eta < 0, \tag{32.c}$$

we readily reach the following conclusions.

(i) For a given pressure P, the first-order transition is reached by fixing η (resp. T) and letting T (resp. η) vary. This first-order transition point reached by allowing one bifurcating parameter to *increase* will be denoted by the subscript "1" and the superscript ">". According to Eqs. (17) and (32.a)–(32.c), k_c (resp. k_3) is a decreasing (resp. increasing) function of T and an increasing function of η (resp. η independent). More specifically, we have (see Fig. 2a)

$$\eta_1^>(P, T_a) > \eta_1^>(P, T_b), \quad T_a > T_b \tag{33.a}$$

and

$$T_1^>(P, \eta_a) > T_1^>(P, \eta_b), \quad \eta_a > \eta_b \tag{33.b}$$

for fixed P.

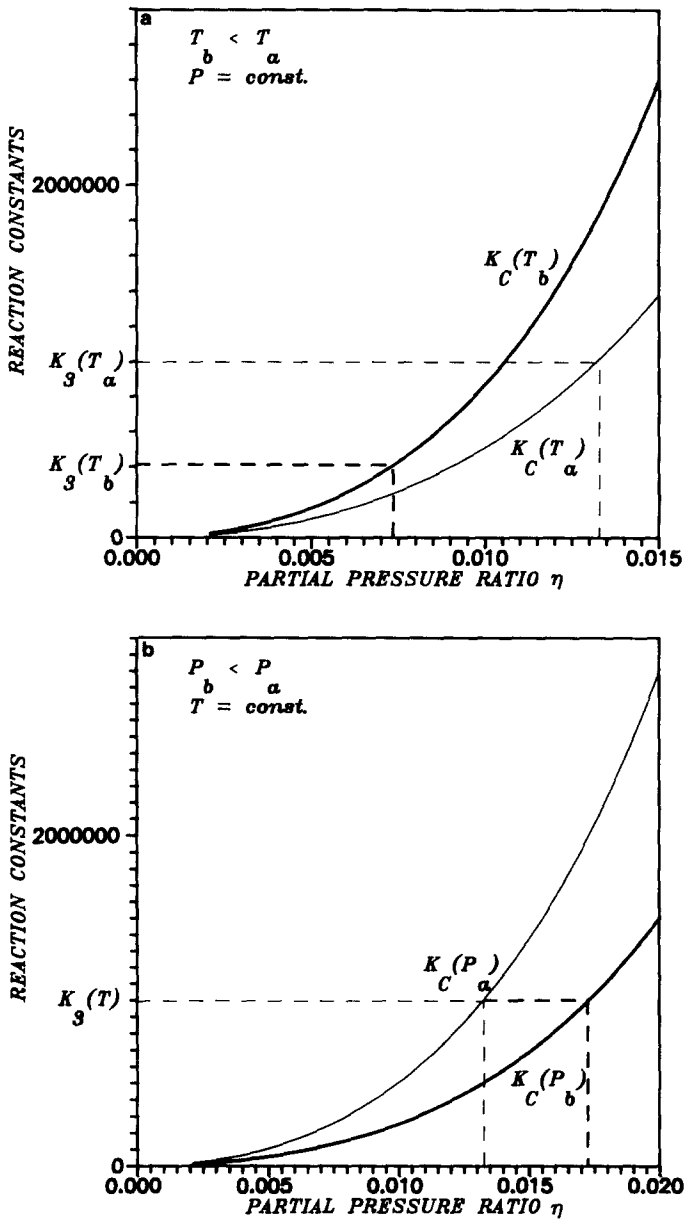

FIG. 2. (a) Effect of the temperature T on the *site*-MFA first-order transition point $\eta_1^>$ at constant pressure P. Here $T_a = 500$ K ($k_3(T_a) = 10^6\ s^{-1}$), $T_b = 450$ K, $P = 1$ atm (see Eqs. (48a)–(48c)). (b) Effect of the pressure P on the *site*-MFA first-order transition point $\eta_1^>$ at constant temperature T. Here $k_3 = 10^6\ s^{-1}$, $T = 500$ K, $P_a = 1$ atm, and $P_b = 0.5$ atm (see Eqs. (48a)–(48c)).

(ii) When, for a given reaction–catalyst system, one lowers the pressure P allowing T (resp. η) to remain unchanged, one observes a shift of the critical value $\eta_1^>$ (resp. $T_1^>$) toward higher (resp. lower) values. Namely, we have (see Fig. 2b)

$$\eta_1^>(P_a, T) < \eta_1^>(P_b, T), \quad P_a > P_b \quad (33.c)$$

for fixed T and, if we fix η, we have

$$T_1^>(P_a, \eta) > T_1^>(P_b, \eta), \quad P_a > P_b. \quad (33.d)$$

3. PAIR MEAN FIELD APPROXIMATION

The kinetics of the pair coverages X_{ij} are related to the triplet coverages X_{ijk} as the reaction scheme involves two neighbouring site mechanisms (Eqs. (2.2)–(2.3)). We derive closed kinetic equations for the X_{ij} by working in the pair-MFA whose underlying ideas have been presented in the Introduction. Practically it consists of inserting in the pair kinetics the following approximate forms for the triplet coverages X_{ijk}:

$$X_{iii} = X_{ii}^2/X_i \tag{34.a}$$

$$X_{iik} = X_{ii}X_{ik}/X_i, \quad i \neq k \tag{34.b}$$

$$X_{iki} = X_{ik}^2/4X_k, \quad i \neq k \tag{34.c}$$

$$X_{ijk} = X_{ij}X_{jk}/2X_j, \quad i \neq j \neq k. \tag{34.d}$$

We report in Appendix A the resulting equations for the X_{ij}. Let us stress that this approach is valid only for $\tau_3 \neq 0$ and cannot be extended to $\tau_3 = 0$ as we do not consider the possibility of instantaneous reaction. The phase diagrams for the irreversible model, Eqs. (2.1)–(2.3), are obtained by gathering the steady-state solutions of Eqs. (A1)–(A6) (with $k_{-1} = k_{-2} = k_4 = 0$) into the sum rules Eq. (8). These bifurcation diagrams have the same form as those of the ZD model (i.e., for $\tau_3 = 0$) (*16*, *17*).

The only significant difference lies in the critical values of the bifurcating parameters at which the adsorbate undergoes a first- and a second-order phase transition. Values of these transition points may be found in Table 1.

TABLE 1

First-Order Transition Point ($Y_1^>$) and Second-Order Transition Point (Y_2), Functions of k_3, Obtained by the Three Different Methods

Y_A	$\tilde{k}_3$	*Site*-MFA	*Pair*-MFA	MC simulations
$Y_1^>$	$\tau_3 = 0$	0.5610 (*17*)	0.5241 (*17*)	0.525 ± 0.001 (*16*)
Y_2		0 (*17*)	0.2497 (*17*)	0.389 ± 0.005 (*16*)
$Y_1^>$	10^6	0.6666	0.60	0.52 ± 0.01
	10	0.5928	0.55	0.52 ± 0.01
	1	0.5	0.46	0.435 ± 0.05
	0.1	0.3025	0.295	0.295 ± 0.05
Y_2	10^6	0	0.25	0.38 ± 0.01
	10	0	0.25	0.38 ± 0.01
	1	0	0.24	0.36 ± 0.01
	0.1	0	0.205	0.285 ± 0.05

In order to allow us a direct comparison between our results (i.e., with k_3 finite) and those of the ZD model (i.e., with $k_3 = \infty$) we must scale the kinetics according to MCS procedure of Ziff *et al.* (*16*). Within this formulation the starting equations ((6.a) and (6.b)) have the dimensionless form

$$\frac{dX_A}{d\tilde{t}} = Y_A X_S - 2\tilde{k}_3 X_{AB} \tag{34.e}$$

$$\frac{dX_B}{d\tilde{t}} = 2Y_B X_{SS} - 2\tilde{k}_3 X_{AB}, \tag{34.f}$$

where

$$Y_A = k_1/(k_1 + k_2), \quad Y_B = 1 - Y_A \tag{35}$$

and, by rule,

$$\tilde{k}_3 = k_3/(k_1 + k_2), \quad \tilde{t} = (k_1 + k_2)t. \tag{36}$$

As in the treatment of Ziff *et al.* (*16*) the probability $Y_A(Y_B)$ represents the relative rate of *potentially efficacious* collisions of molecules $A(B_2)$ with the surface. Although necessary for our comparison this scaling is rather tricky. It involves Y_A and $\tilde{k}_3$ as bifurcating parameters, the use of which requires some comments.

(i) By definition, the two parameters Y_A and $\tilde{k}_3$ are coupled and contain the three bifurcating parameters η, T, and P (use Eqs. (16.a)–(16.e)):

$$Y_A = \eta/(\eta + \alpha_T) \tag{37}$$

$$\tilde{k}_3 = k_3(1 + \eta)/[\tilde{k}_1 P(\alpha_T + \eta)]. \tag{38}$$

(ii) When formulated in terms of Y_A and $\tilde{k}_3$ the *site*-MFA condition for the first-order transition, Eq. (29), reads ($Y_1^> = Y_c$ here)

$$2Y_c^3 - (2 - 9\tilde{k}_3)Y_c^2 - 12\tilde{k}_3 Y_c + 4\tilde{k}_3 = 0. \tag{39}$$

(iii) In order to find the value for the triplet of adjustable parameters $\{\eta, T, P\}$ corresponding to a given value of the couple $\{Y_A, \tilde{k}_3\}$ one can proceed as follows. For a given value of $\tilde{k}_3$, i.e., a combination of values (so

far unspecified) for $\{\eta, T, P\}$, a given value of Y_A can be related to some couple of values for $\{\eta, T\}$ by using Eq. (37), namely,

$$\eta = \alpha_T Y_A/(1 - Y_A), \quad \text{for } T \text{ fixed} \quad (40)$$

or (use Eq. (16.e))

$$T = (E_2 - E_1)/R\{ln\ \alpha_\infty - ln\ \eta + ln[Y_A/(1 - Y_A)]\}, \quad \text{for } \eta \text{ fixed.} \quad (41)$$

Then for this couple of values for $\{\eta, T\}$ one can reach the corresponding value of P by means of Eq. (38).

Now if we examine the *pair*-MFA results reported in Table 1 we reach a principal conclusion. Compared to the *site*-MFA, the *pair*-MFA shows a new steady-state property of the irreversible model, Eqs. (2.1)–(2.3), namely, a second-order phase transition (i.e., continuous) which appears for a *finite* value Y_2 of the bifurcating parameter Y_A. The physical meaning of this second-order phase transition is the following. In the region of small Y_A (i.e., η) the surface is mainly occupied by atoms $B(Y_B \gg Y_A)$. In most cases when a molecule A adsorbs, it has a nearest neighbour of type B and therefore, after some time, on the average τ_3, desorbs within a product molecule AB. Although a finite *transient* reaction rate exists, the steady-state reaction rate $\bar{R}_3$ remains zero (i.e., $\bar{X}_B = 1$ and $\bar{X}_A = 0$) up to a critical value $Y_A = Y_2$ where it begins to increase continuously to a maximum value reached when $Y_A = Y_1^>$ beyond which it drops to zero.

In other words, when treated within the *pair*-MFA, the irreversible model, Eqs. (2.1)–(2.3), present a *reactive window* for Y_A such that

$$Y_2 \leq Y_A \leq Y_1^>. \quad (42)$$

As shown in Table 1, the width of this reactive window clearly depends on $\tilde{k}_3$. We observe that when $\tilde{k}_3$ decreases, $Y_1^>$ shifts substantially toward smaller values with, as a result, a narrowing of the reactive window. Indeed, when

$$k_3 < k_1 + k_2, \quad (43)$$

i.e., when the reaction mechanism Eq. (2.3), becomes the rate-limiting step of the reaction, Eq. (1), this narrowing of the reactive region becomes crucial.

In relation to this curious feature of the irreversible model for the reaction of Eq. (1), let us briefly consider the sister reaction

$$A + B \xrightarrow{\text{catalytic surface}} AB, \quad (44)$$

where neither A nor B dissociates upon adsorption.

The exact kinetic equations for the irreversible model of this reaction, Eq. (44), have the form

$$dX_A/dt = k_1 X_S - R_3 \quad (45.a)$$

$$dX_B/dt = k_2 X_S - R_3. \quad (45.b)$$

The steady-state equation

$$(k_1 - k_2)\bar{X}_S = 0 \quad (46)$$

implies that $\bar{X}_S$ is not zero (and $\bar{R}_3 \neq 0$) only when $k_1 = k_2$. Therefore the reactive window is reduced to the single point $Y_A = 0.5$; otherwise the surface is poisoned by species A (resp. B) when $Y_A > 0.5$ (resp. $Y_A < 0.5$). This well-known feature of the reaction of Eq. (44), (e.g., see Ref. (*19b*)) is confirmed by MCS (*16*).

It appears that when operating in the regime of Eq. (43), our reaction, Eq. (1), tends to behave like its sister reaction, Eq. (44). Indeed for $\tilde{k}_3 < 1$, the *pair*-MFA shows that the two-site rule for adsorption of B_2 involves a steady-state coverage function $\bar{X}_{SS}$ which departs from its *site*-MFA expression $\bar{X}_S^2$ as follows:

$$\bar{X}_{SS} = \bar{X}_S^{[2-\gamma\tilde{k}_3]}. \quad (47)$$

This feature, already pointed out by previous MC simulations (*22*), is illustrated in Fig. 3 which represents γ, function of η, in the reactive window $[\eta_2, \nu_1^>]$ for $\tilde{k}_3 \approx 0.1$. This plot clearly shows that $\bar{X}_S$ approaches its *site*-MFA value $\bar{X}_S^2$ when $\eta \to \eta_1^>$ while for $\eta \to \eta_2$, $\bar{X}_{SS}$ behaves rather as $\bar{X}_S$.

Note that the existence of a second-order transition as well as this narrowing of the reactive window observed (in the absence

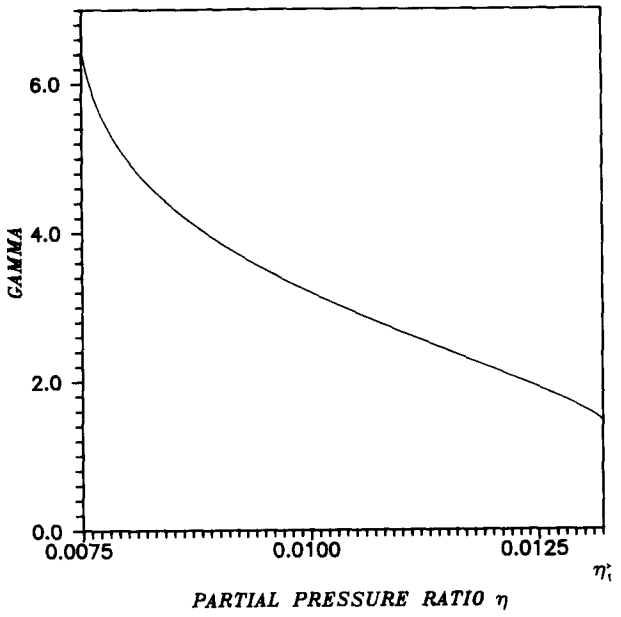

FIG. 3. Plot of γ, Eq. (47), vs η in the reactive window $[\eta_2, \eta_1^>] = [0.0073, 0.0132]$ for the CO oxidation at $P = 1$ atm and $T = 500$ K (see Fig. 5). Note that at $\eta = \eta_2 + \varepsilon$, $\tilde{k}_3 = 0.104$ and $X_{SS} = X_S^{1.32}$ while for $\eta = \eta_1^>$, $k_3 = 0.091$ and $X_{SS} = X_S^{1.87}$.

of any desorption) in the *pair*-MFA are confirmed by the MCS results we present in the next section.

4. RESULTS AND DISCUSSION

The first results concern the irreversible model, Eqs. (2.1)–(2.3), and are reported in Table 1. In our MCS investigations we assign to the steady-state coverages $\overline{X}_A$, $\overline{X}_B$ the values that, once reached by the system, remain constant within a margin of 1%. These MCS investigations have been performed by fixing $\tilde{k}_3$ and allowing the bifurcating parameter Y_A to vary (see Section 3). Table 1 gives the critical value $Y_1^>(Y_2)$ of Y_A which corresponds to the first (second)-order phase transition for different values of $\tilde{k}_3$.

The examination of Table 1 leads to the following remarks:

(i) It is only for $\tilde{k}_3 \leq 1$ that our MCS values of $Y_1^>$ and Y_2 differ from those obtained by Ziff *et al.* (*16*).

(ii) For $\tilde{k}_3 \leq 1$ the values of $Y_1^>$ in the *pair*-MFA (and even in the *site*-MFA) are in a fairly good agreement with the MCS values. This is not surprising. For $Y_A \to Y_1^>$ the reactant coverages become comparable ($\overline{X}_A \approx \overline{X}_B$) and for $k_3 \leq k_1 + k_2$ enough *AB* pairs remain on the surface to favor a random mixing of the species *A* and *B* (see also Eq. (47)). On the contrary, in the ZD model $X_{AB} = 0$ and the adsorbate is only made of isolated clusters (constituted of molecules *A* or *B* exclusively) which are rather compact (desorption processes are excluded in this model).

(iii) The case of Y_2 is different. The pair-MFA clearly underestimates Y_2 with respect to the MCS. Note also that when $\tilde{k}_3 \approx 0.1$ the reactive window $[Y_2, Y_1^>]$ almost shrinks. This curious feature has been discussed in Section 3.

Let us also add here that in the presence of *A*-desorption, Eq. (3), the transition point $Y_1^>$ shifts to higher values while Y_2 remains almost unchanged. For instance, for $\tilde{k}_3 = 1$ and $k_{-1} = 0.1k_3$ the *pair*-MFA gives $Y_1^> = 0.525$ and $Y_2 = 0.24$ while MCS lead to $Y_1^> = 0.51 \pm 0.01$ and $Y_2 = 0.38 \pm$

0.01 (compare with Table 1). For more realistic (i.e., lower) values of k_{-1} the shift of $Y_1^>$ is less important.

The results we present now are illustrative of our case study, i.e., CO oxidation under atmospheric pressure and for $T \leq 500$ K. If, in this regime, isothermal conditions could not strictly be established, this is not crucial. Indeed, we only consider steady states, i.e., with a "surface temperature" $\bar{T}_S$ constant and a few degrees above the ambient temperature T (*19*). Unless otherwise specified we refer to the following indicative values (see Section 2 for definitions)

$$\bar{k}_1 = 5.433 \times 10^9\, T^{-1/2} \tag{48.a}$$

$$\bar{k}_2 = 3.576 \times 10^9\, T^{-1/2} \exp(-1500/T) \tag{48.b}$$

$$k_3 = k_3' \exp(-4000/T) \tag{48.c}$$

$$k_{-1} = k_{-1}' \exp(-12500/T) \tag{48.d}$$

$$k_4 = (\sigma_{ER}/\sigma_1) k_1. \tag{48.e}$$

In these formulae, we fix $N = 5.10^{14}$ sites cm^{-2}; the pressures are in atmospheres and the activation energies in degrees K. Moreover, we use $\sigma_1 = 0.54$, $\sigma_2 = 0.38$ (*23*); $E_1 = 0$, $E_2 = 3$ kcal mole^{-1} (*24*); $k_3' \approx 10^9$ s^{-1}, $E_{-1} = 25$ kcal mole^{-1} (*24*). Finally we describe the Eley–Rideal mechanism, Eq. (4), of "cross section" σ_{ER}, by the usual collisional model for the CO adsorption.

With these values of $\bar{k}_1$, $\bar{k}_2$, and for $\eta \approx 1\%$, $T \approx 500$ K, Eq. (38) yields the following value for the reaction time τ_3

$$\tau_3 = k_3^{-1} \approx 10^{-7}/\tilde{k}_3 P. \tag{49}$$

Therefore at $P \approx 1$ atm, we have

$$k_3 \approx 10^6 \text{ s}^{-1}, \text{ i.e., } \tilde{k}_3 \approx 0.1. \tag{50}$$

These values are consistent with the experimental turnover number (averaged over the reactive window), i.e., a few hundred molecules per second per site (*5*) and with the *site*-MFA critical constant $k_c \approx 5.10^3$ s^{-1} (use Eq. (24)).

The reaction has been MC-simulated without any reduction in the rate constants and we choose the partial pressure ratio $\eta = p_1/p_2$ as bifurcating parameter ($P = 1$ atm, $T \approx 500$ K).

The most significant results are represented in Figs. 4–7. We have only plotted the bifurcating diagram for the steady state coverage $\bar{X}_A$ (i.e., $\bar{X}_{CO}$) for different situations. The qualitative corresponding behaviour of the companion coverages $\bar{X}_B$ (i.e., $\bar{X}_0$) may readily be guessed from these figures (e.g., see Fig. 1).

The examination of Figs. 4–7 leads to the following remarks:

(i) As $k_3 \approx 0.1$, the site-MFA is sufficient to localize the first-order transition point $\eta_1^>$ (see Fig. 4).

(ii) The second-order phase transition is "killed" (i.e., $\eta_2 = 0$) by the ER mechanism, Eq. (4) (see Fig. 5). Note that this vanishing of the second-order transition has been observed, in the *pair*-MFA, for values of σ_{ER}/σ_1, Eq. (48.e), as small as 5.10^{-4}. The ER mechanism also causes a small shift of the transition point $\eta_1^>$ toward smaller values.

(iii) When finite (i.e., when $k_4 = 0$), η_2 should be determined by MCS rather than within the *pair*-MFA (see Figs. 4–6).

(iv) As is well-known, a steady-state hysteresis occurs only when CO desorbs (see Figs. 6 and 7). In this situation an additional critical point appears at $\eta = \eta_1^<$ marking out the first-order transition from a stable adsorbate pure in CO ($\bar{X}_{CO} \lesssim 1$, $\bar{X}_0 = 0$) to a stable mixed adsorbate richer in oxygen ($\bar{X}_0 > \bar{X}_{CO} > 0$). Experimentally one reaches $\eta_1^<$ by allowing η to *decrease*, while on the contrary, $\eta_1^>$ is determined by allowing η to *increase*. Note that the first-order transition point $\eta_1^<$ (out of reach by MCS) should better be determined within the *pair*-MFA than within the *site*-MFA. For instance, with $k_{-1}' = 10^{15}$ s^{-1}, the *pair* (resp. *site*)-MFA gives $\eta_1^< = 0.0098$ (resp. $\eta_1^< = 0.0037$). Finally let us mention that, in the *pair*-MFA, we have observed hysteresis for values of k_{-1}' as small as 10^{11} s^{-1}.

(v) If present, the second-order transition point η_2 should be experimentally

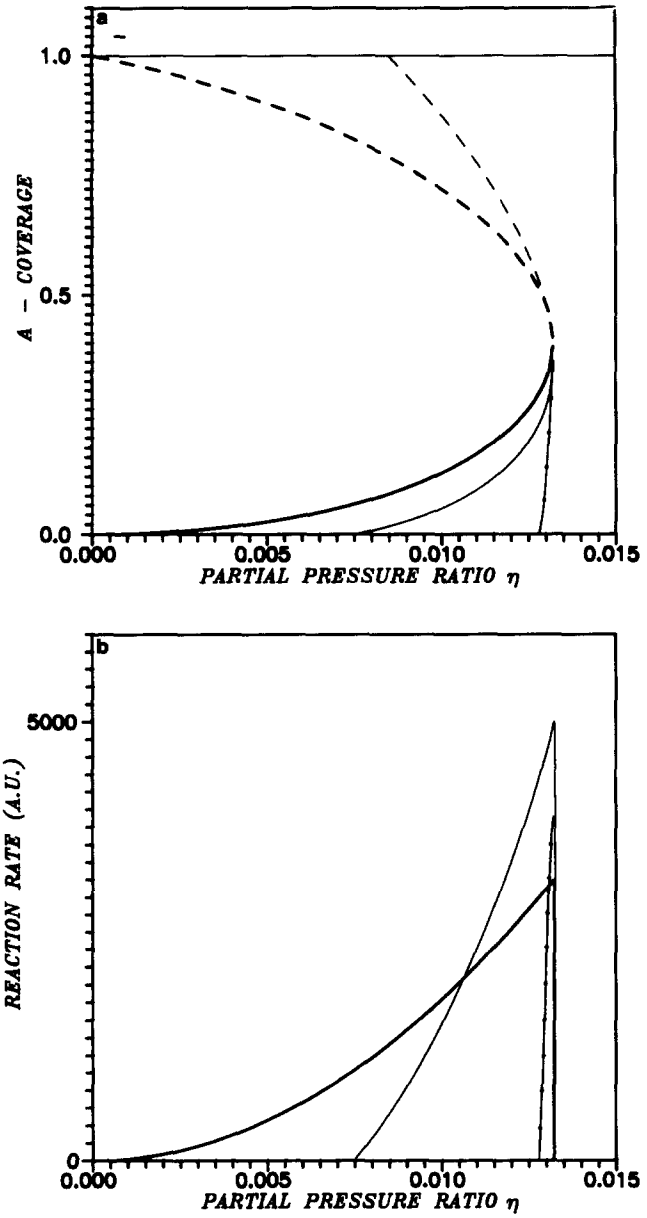

FIG. 4. Bifurcating diagram for $\overline{X}_A$ for the irreversible model (i.e., $k_{-1} = k_4 = 0$). The heavy line represents the *site*-MFA result: $\eta_2 = 0$, $\eta_1^> = 0.0132$. The thin line represents the *pair*-MFA result: $\eta_2 = 0.0073$, $\eta_1^> = 0.132$. The third line (—·—) represents the MCS result: $\eta_2 = 0.0127$, $\eta_1^> = 0.0133$. The dashed lines represent the unstable steady states. The unstable branch ($\overline{X}_A > \overline{X}_B$) is out of reach by MCS. The reactive window is narrowed by MC simulation as seen in the lowest part (b) which shows the corresponding steady-state reaction rates.

marked out by measuring the steady-state reaction rate hysteresis. (Compare Figs. 6b and 7b)

5. CONCLUSIONS

We have reported and analysed steady-state features such as bifurcation diagrams

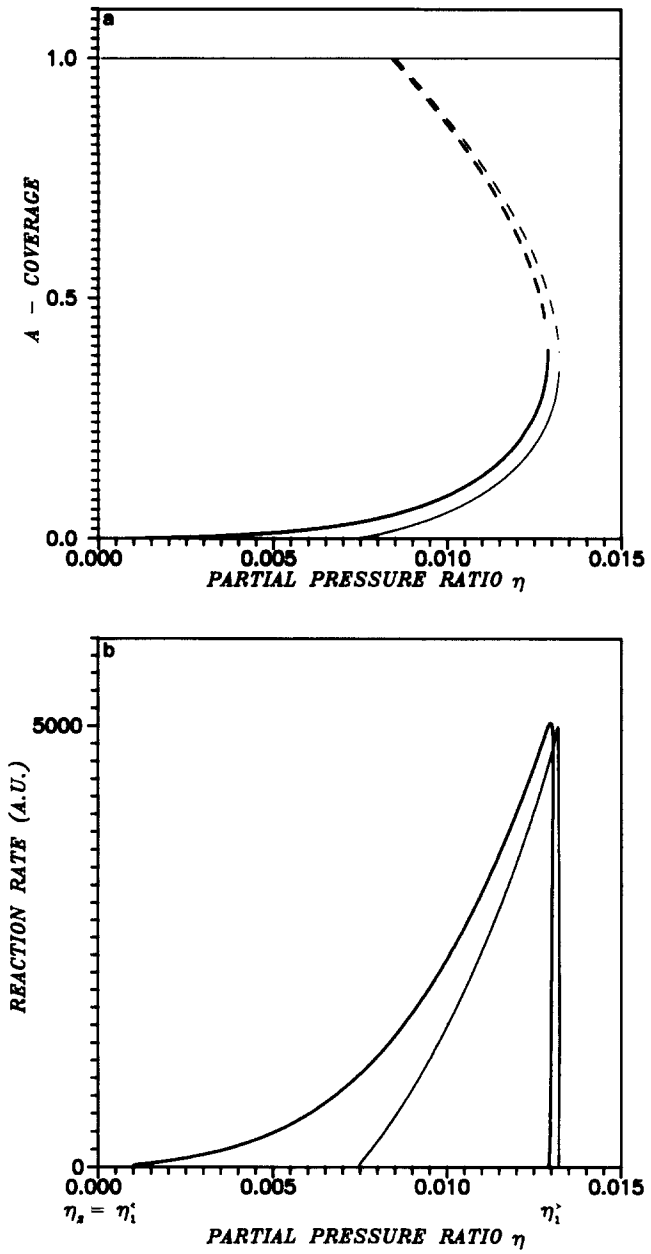

FIG. 5. (a) *Pair*-MFA bifurcating diagram for $\bar{X}_A$: effect of the ER mechanism. The thin line corresponds to the case $k_{-1} = k_4 = 0$: $\eta_1^< = 0$, $\eta_2 = 0.0073$, $\eta_1^> = 0.0132$; MC simulation gives $\eta_2 = 0.0127$. The heavy line corresponds to the case $k_{-1} = 0$, $k_4 = 10^{-2}k_1$: $\eta_1^< = \eta_2 = 0$, $\eta_1^> = 0.0128$; this result is confirmed by MCS. The dashed lines represent the unstable steady states. (b) *Pair*-MFA steady-state reaction rate $\bar{R}_3$ corresponding to these cases.

and reaction rate hysteresis for the bimolecular surface reaction, Eq. (1). These results have been obtained by means of statistical methods (the *site*- and *pair*-MFA) and using our MC simulation procedures for such surface reactions.

Our first conclusion concerns the influence of a *finite* reaction rate constant on the

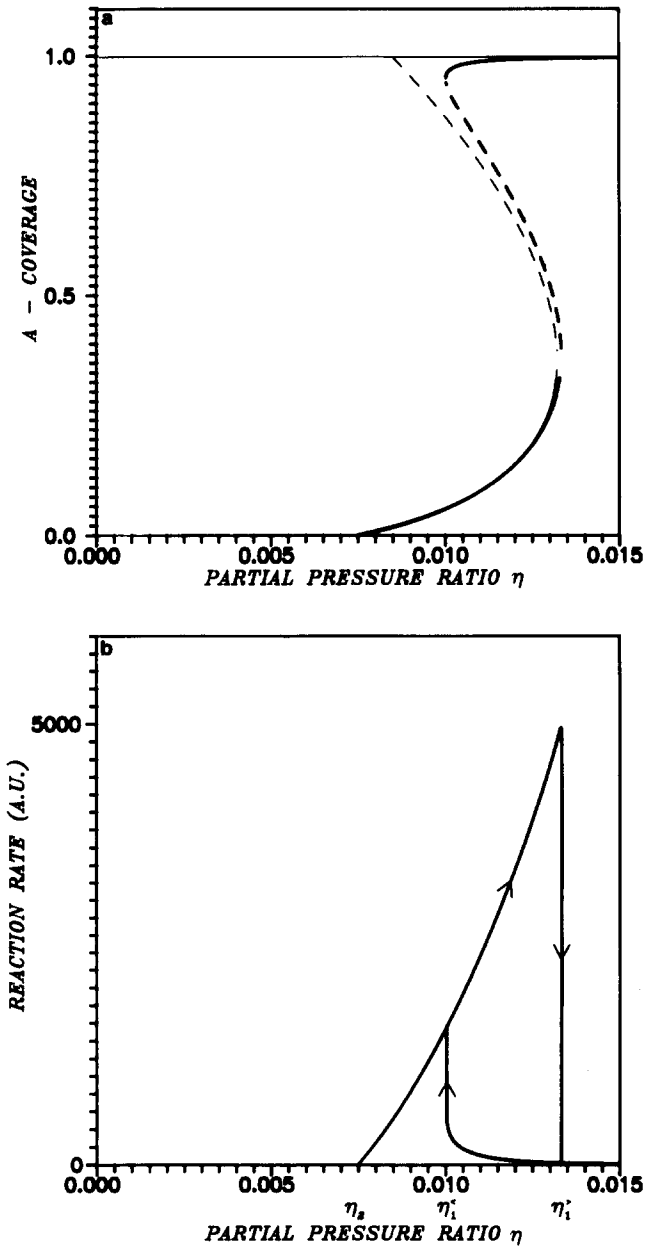

FIG. 6. (a) *Pair*-MFA bifurcating diagram for $\overline{X}_A$: effect of the desorption of A. The thin line corresponds to the case $k_{-1} = k_4 = 0$ (see Fig. 5). The heavy line corresponds to the case $k_{-1} = 1.39 \times 10^{-4}$, $k_4 = 0$: $\eta_2 = 0.0073$, $\eta_1^< = 0.0098$, $\eta_1^> = 0.0134$. MCS gives $\eta_2 = 0.00127$. The dashed lines represent unstable steady states. (b) *Pair*-MFA steady-state reaction rate hysteresis (case: $k_{-1} \neq 0$, $k_4 = 0$). Compare with Fig. 7b.

bifurcation diagram of the irreversible model, Eqs. (2.1)–(2.3). In 1986, Ziff *et al.* (*16*), by MC simulations, and Dickman (*17*), in the *pair*-MFA, have shown that for an *infinite* reaction rate constant this bifurcation diagram presents two kinetic phase

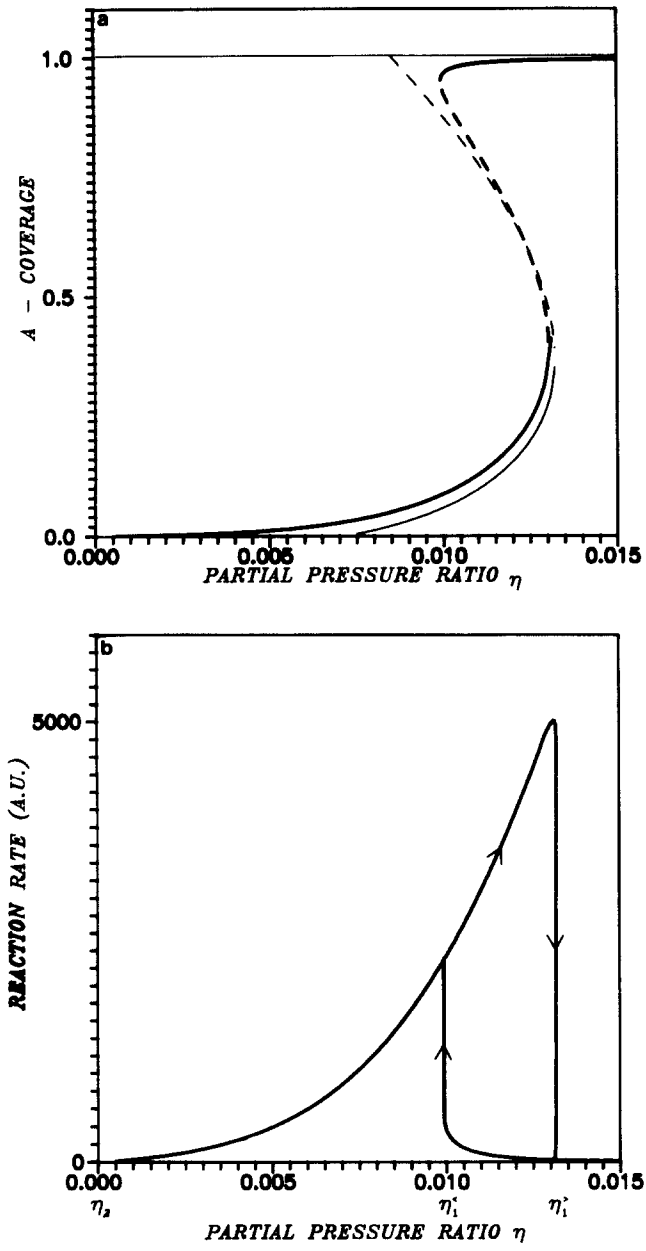

FIG. 7. (a) *Pair*-MFA bifurcating diagram for $\overline{X}_A$: effect of ER and A-desorption mechanisms. The thin line corresponds to the case $k_{-1} = k_4 = 0$ (see Fig. 5). The heavy line corresponds to the case $k_{-1} = 1.39 \times 10^4$, $k_4 = 10^{-2}k_1$: $\eta_2 = 0$, $\eta_1^< = 0.0098$, $\eta_1^> = 0.0129$. The dashed line represent unstable steady states. (b) *Pair*-MFA steady-state reaction rate hysteresis (case: $k_{-1} \neq 0$, $k_4 \neq 0$). Compare with Fig. 6b.

transitions. Namely, in terms of the bifurcating parameter Y_A, Eq. (35),

(i) a first-order transition, at $Y_A = Y_1^>$, which characterizes the sudden jump from the maximum reactive state to the "poisoning" (saturation) of the surface by species A, and

(ii) a second-order transition, at $Y_A = Y_2$, where the pure B-adsorbate

smoothly changes into a mixed adsorbate with, as a result, the starting of the reaction.

Therefore, the reaction proceeds only in the "reactive window" Y_A: $[Y_2, Y_1^>]$. This reactive phase is enclosed between two inhibited phases: the surface is poisoned by the species B (resp. A) when $Y < Y_2$ (resp. $Y > Y_1^>$).

We obtain results comparable to those of Ziff *et al.* and Dickman (*16, 17*), as far as we consider situations where the adsorption processes, Eqs. (2.1) and (2.2), are the rate-limiting steps of the reaction, i.e., at low pressure P. However, we have observed that when $\tilde{k}_3 \to 1$ (see Eq. (36)) the reactive window narrows and almost shrinks when the reaction step, Eq. (2.3), becomes the rate-limiting process of the reaction, i.e., for pressure P in the atmospheric range. This critical narrowing is due to the existence of the second-order phase transition.

Our second conclusion concerns the modifications of the bifurcation diagram and the steady-state reaction rate of the reaction when we add to the basic model, Eqs. (2.1)–(2.3), the desorption, Eq. (3), and/or the ER mechanism, Eq. (4). Here we express these properties by considering the partial pressure ratio η as the only adjustable bifurcating parameter of the problem (i.e., we fix P and T).

When we add to the irreversible model, Eqs. (2.1)–(2.3), the desorption of A, Eq. (3), we observe an additional first-order phase transition, at $\eta = \eta_1^<$. At this transition point the system jumps from a stable steady-state adsorbate very rich in $A(\bar{X}_A \gg \bar{X}_B)$ to a stable steady-state adsorbate richer in $B(\bar{X}_A < \bar{X}_B)$. In the interval $[\eta_1^<, \eta_1^>]$ the system is bistable and, as a consequence, we observe a steady-state reaction rate hysteresis. Note also that, in the absence of the ER mechanism, Eq. (4), this first-order transition point $\eta_1^<$ is "pushed" by the second-order transition (at $\eta = \eta_2$) toward the other first-order transition point $\eta_1^>$. This is normal as in the steady states such that $\eta < \eta_2$ there is no species A on the surface $(\bar{X}_A = 0)$.

When we add to the irreversible model, Eq. (2.1)–(2.3), the ER mechanism, Eq. (4), we observe, as expected, the vanishing of the second-order kinetic phase transition (i.e., $\eta_2 \to 0$) and a broadening of the reactive window which becomes $[0, \eta_1^>]$. This feature has been observed for values of $\sigma_{ER}/\sigma_1 > 10^{-5}$ (see Eq. (5)).

When we add to the irreversible model, Eqs. (2.1)–(2.3), both the desorption of A, Eq. (3), and the ER mechanism, Eq. (4), we observe the vanishing of the second-order phase transition ($\eta_2 \to 0$). There results, as above, a broadening of the reactive window which becomes $[0, \eta_1^>]$ and, also important, a shift of the first-order transition point $\eta_1^<$ toward smaller values of η, i.e., a significant broadening of the "bistability window" $[\eta_1^<, \eta_1^>]$.

The problem of the second-order kinetic phase transition (at η_2) requires some final comments.

(i) To our knowledge, there is no experimental evidence of such a second-order transition. The reaction rate begins to increase as soon as η departs from zero (e.g., Ref. (*5b*)).

(ii) The second-order transition observed for η_2 finite is an artifact of the model. According to our assumptions (1) and (2) (see Introduction) the surface is made of active sites (of the same kind) which are invariably compatible for the adsorption of both gaseous reactants. In this case the saturation of the surface with reactant B (e.g., oxygen) necessarily precludes the adsorption of the companion reactant A (e.g., CO). Therefore if the LH mechanism, Eq. (2.3), is the unique reaction step, it is normal that for low values of η, the steady-state reaction rate vanishes. It is also obvious that if the ER mechanism, Eq. (4), is also involved in the model this second-order transition disappears ($\eta_2 \to 0$).

(iii) If the surface was composed of two kinds of sites, e.g., sites "α" (resp. "β") compatible for the adsorption of A and B_2

(resp. only of A), even if the LH mechanism, Eq. (2.3), were the unique reaction step, the second-order transition would clearly disappear, i.e., $\eta_2 \to 0$. The β sites can be interpreted in the Ertl model (*7*) as the sites of the hex phase while in the STM model (*8*) as those blocked by oxide formation.

It thus would appear that the lack of observation of a second-order kinetic phase transition is of little use in the discussion of the controversial role of the ER mechanism in the CO oxidation kinetics, for instance (e.g., Refs. (*26, 27*)).

However, this absence of a second-order transition, when explained, will present an advantage in heterogeneous catalysis where one considers surface reactions operating at ordinary pressures, i.e., when $k_3 \leq 1$. Indeed, in this case we have seen that pair MFA equations would be sufficient to investigate the steady-state features of these reactions in their reactive and bistability windows ($[0, \eta_1^>]$ and $[\eta_1^<, \eta_1^>]$, respectively).

APPENDIX A: THE PAIR EQUATIONS

We consider the reaction, Eq. (1), described in the kinetic scheme, Eqs. (2.1)–(2.3), (3), and (4), completed by the associative desorption of atoms B, i.e.,

$$B_2 + S_2 \xleftarrow{-2} 2\,BS.$$

Using the *pair*-MFA, sketched in Section 3 (See Eqs. (34a)–(34d)), we derive for the pair coverages X_{ij}, Eq. (5), the following kinetic equations:

$$\begin{aligned}\frac{dX_{AS}}{dt} &= 2k_1X_{SS} - k_1X_{AS} - \tfrac{3}{2}k_2\frac{X_{AS}X_{SS}}{X_S} \\ &\quad + \tfrac{3}{2}k_3\frac{X_{AB}^2}{X_B} + 3k_3\frac{X_{AA}X_{AB}}{X_A} \\ &\quad - \tfrac{3}{2}k_3\frac{X_{AB}X_{AS}}{X_A} + 2k_{-1}X_{AA} \\ &\quad - k_{-1}X_{AS} + k_4X_{AB} + 3k_{-2}\frac{X_{AB}X_{BB}}{X_B}\end{aligned} \tag{A.1}$$

$$\begin{aligned}\frac{dX_{BS}}{dt} &= 3k_2\frac{X_{SS}^2}{X_S} - \tfrac{3}{2}k_2\frac{X_{BS}X_{SS}}{X_S} - k_1X_{BS} \\ &\quad - \tfrac{3}{2}k_3\frac{X_{AB}X_{BS}}{X_B} + \tfrac{3}{2}k_3\frac{X_{AB}^2}{X_A} \\ &\quad + 3k_3\frac{X_{BB}X_{AB}}{X_B} + k_{-1}X_{AB} \\ &\quad + 2k_4X_{BB} - k_4X_{BS} + 6k_{-2}\frac{X_{BB}^2}{X_B} \\ &\quad - 3k_{-2}\frac{X_{BB}X_{BS}}{X_B}\end{aligned} \tag{A.2}$$

$$\begin{aligned}\frac{dX_{AB}}{dt} &= k_1X_{BS} + \tfrac{3}{2}k_2\frac{X_{AS}X_{SS}}{X_S} - \tfrac{3}{2}k_3\frac{X_{AB}^2}{X_B} \\ &\quad - \tfrac{3}{2}k_3\frac{X_{AB}^2}{X_A} - k_3X_{AB} - k_{-1}X_{AB} \\ &\quad - k_4X_{AB} - 3k_{-2}\frac{X_{AB}X_{BB}}{X_B}\end{aligned} \tag{A.3}$$

$$\frac{dX_{AA}}{dt} = k_1X_{AS} - 3k_3\frac{X_{AA}X_{AB}}{X_A} - 2k_{-1}X_{AA} \tag{A.4}$$

$$\begin{aligned}\frac{dX_{BB}}{dt} &= \tfrac{1}{2}k_2X_{SS} - 3k_3\frac{X_{BB}X_{AB}}{X_B} \\ &\quad + \tfrac{3}{2}k_2\frac{X_{BS}X_{SS}}{X_S} - 2k_4X_{BB} - k_{-2}X_{BB} \\ &\quad - 6k_{-2}\frac{X_{BB}^2}{X_B}\end{aligned} \tag{A.5}$$

$$\begin{aligned}\frac{dX_{SS}}{dt} &= -2k_1X_{SS} - \tfrac{1}{2}k_2X_{SS} - 3k_2\frac{X_{SS}^2}{X_S} \\ &\quad + k_3X_{AB} + \tfrac{3}{2}k_3\frac{X_{AS}X_{AB}}{X_A} \\ &\quad + \tfrac{3}{2}k_3\frac{X_{AB}X_{BS}}{X_B} + k_{-1}X_{AS} + k_4X_{BS} \\ &\quad + k_{-2}X_{BB} + 3k_{-2}\frac{X_{BB}X_{BS}}{X_B}\end{aligned} \tag{A.6}$$

Note that, if we collect these pair-equations, Eqs. (A.1)–(A.6), according to Eq. (8), we obtain the following kinetic equations for the coverages X_i:

$$\begin{aligned}\frac{dX_A}{dt} &= R_1 - R_{-1} - R_3 = k_1X_S \\ &\quad - k_{-1}X_A - 2k_3X_{AB}\end{aligned} \tag{A.7a}$$

$$\frac{dX_B}{dt} = 2R_2 - 2R_{-2} - R_3 - R_4 = 2k_2X_{SS} - 4k_{-2}X_{BB} - 2k_3X_{AB} - k_4X_B \quad \text{(A.7b)}$$

and we verify the sum rule, Eq. (7), i.e.,

$$\frac{dX_S}{dt} = -\frac{dX_A}{dt} - \frac{dX_B}{dt}.$$

Eqs. (A.7a) and (A.7b) are *formally* identical to the exact equations for the complete kinetic scheme.

ACKNOWLEDGMENTS

We thank Dr. J. P. Dauchot and Dr. J. P. Dath for their courteous advice about the experimental aspects of the problem.

REFERENCES

1. Nicolis, G., and Prigogine, I., "Self-Organization in Nonequilibrium Systems." Wiley–Interscience, New York, 1977.
2. (a) Schmitz, R. A., D'Netto, G. A., Razon, L. F., and Brown, J. R., *in* "Chemical Instabilities" (G. Nicolis and F. Baras, Eds.), NATO ASI Series C, Vol. 120. Reidel, Dordrecht, 1984). (b) Kaul, D. J., and Wolf, E. E., *J. Catal.* **91,** 216 (1985) and **93,** 321 (1985).
3. Schwartz, S. B., and Schmidt, L. D., *Surf. Sci.* **183,** L269 (1987).
4. Razon, L. F., and Schmitz, R. A., *Catal. Rev. Sci. Eng.* **28,** 89 (1986).
5. (a) See, for instance, Golchet, A., and White, J. M., *J. Catal.* **53,** 266 (1978); Barkowski, D., Haul, R., and Kretschmer, U., *Surf. Sci.* **107,** L329 (1981); Dauchot, J. P., and Dath, J. P., *J. Catal.* **86,** 373 (1984); Bolten, H., Hahn, T., Le Roux, J., and Lintz, H. G., *Surf. Sci.* **160,** L529 (1985). (b) Dath, J. P., PhD thesis, Mons University (1988).
6. Slin'ko, M. G., and Slin'ko, M. M., *Catal. Rev. Sci. Eng.* **17,** 119 (1978).
7. (a) Imbihl, R., Cox, M. P., Ertl, G., Müller, H., and Brenig, W., *J. Chem. Phys.* **83,** 1578 (1985); (b) Imbihl, R., Cox, M. P., and Ertl, G., *J. Chem. Phys.* **84,** 3519 (1986); (c) Möller, P., Wertzl, K., Eiswirth, M., and Ertl, G., *J. Chem. Phys.* **85,** 5328 (1986).
8. Sales, B. C., Turner, J. E., and Maple, M. B., *Surf. Sci.* **114,** 381 (1982).
9. Yates, R. C., Turner, J. E., Sallmann, A. J., and Somorjai, G. A., *Surf. Sci.* **149,** 175 (1985).
10. Burrows, V. A., Sundaresan, S., Chabal, Y. J., and Christman, S. B., *Surf. Sci.* **160,** 122 (1985).
11. Cutlip, M. B., *AIChE J.* **25,** 502 (1979).
12. Graham, W. R. G., and Lynch, D. T., AIChE Annual Meeting, Chicago Nov., 1985, Paper 132a.
13. (a) Zhou, X., and Gulari, E., *Chem. Eng. Sci.* **41,** 883 (1986); (b) Zhou, X., Barshad, Y., and Gulari, E., *Chem. Eng. Sci.* **41,** 1277 (1986).
14. (a) Dumont, M., and Dagonnier, R. *in* "Interface under Laser Irradiation" (L. D. Laude, D. Bänerle, and M. Wautelet, Eds.), NATO ASI Series E, Vol. 134. Nijhoff, Dordrecht, 1987. (b) Dumont, M., and Dufour, P., *Comput. Phys. Comm.* **41,** 1 (1986). (c) Dufour, P., Dumont, M., Chabart, V., and Lion, J., *Comput. Chem.* **13,** 25 (1989).
15. Clark, A., "The Theory of Adsorption and Catalysis." Academic Press, New York, 1970.
16. Ziff, R. M., Gulari, E., and Barshad, Y., *Phys. Rev. Lett.* **56,** 2553 (1986).
17. Dickman, R., *Phys. Rev. A* **34,** 4246 (1986).
18. Burley, D. M., *in* "Phase Transitions and Critical Phenomena" (C. Domb and J. Lebowitz, Eds.), Vol. 2. Academic Press, New York, 1972.
19. (a) Dagonnier, R., and Nuyts, J., *J. Chem. Phys.* **65,** 2061 (1976); (b) Dagonnier, R., Dumont, M., and Nuyts, J., *J. Catal.* **66,** 130 (1980).
20. Meakin, P., and Scalapino, D. J., *J. Chem. Phys.* **87,** 731 (1987).
21. Chopard, B., and Droz, M., *J. Phys. A* **21,** 205 (1988).
22. Dumont, M., Poriaux, M., and Dagonnier, R., *Surf. Sci.* **169,** L307 (1986).
23. Kasemo, B., and Törqvist, E., *Phy. Rev. Lett.* **44,** 1555 (1980).
24. Engel, T., and Ertl, G., *in* "Advances in Catalysis" (D. D. Eley, H. Pines, and P. B. Weisz, Eds.), Vol. 28, p. 1. Academic Press, New York, 1979; and *in* "The Chemical Physics of Solid Surfaces and Heterogeneous Catalysis" (D. A. King, and D. P. Woodruff, Eds.), Vol. 4, Chap. 3. Elsevier, Amsterdam, 1982.
25. Bonzel, H. P., and Burton, J. J., *Surf. Sci.* **52,** 223 (1975).
26. Bernasek, S. L., and Somorjai, G. A., *Surf. Sci.* **48,** 204 (1975).
27. Engel, T., and Ertl, G., *Chem. Phys. Lett.* **54,** 95 (1978).